Electrical Structure of the Lithosphere From Rio de la Plata Craton to Paraná Basin: Amalgamation of Cratonic and Refertilized Lithospheres in SW Gondwanaland

M. S. Bologna[1] (ID), G. N. Dragone[1] (ID), R. Muzio[2], E. Peel[2] (ID), P. Nuñez-Demarco[2,3] (ID), and N. Ussami[1] (ID)

[1]Instituto de Astronomia, Geofísica e Ciências Atmosféricas, Departamento de Geofísica, Universidade de São Paulo, São Paulo, Brazil, [2]Instituto de Ciencias Geológicas, Facultad de Ciencias, Universidad de la República, Montevideo, Uruguay, [3]Departamento de Ciencias Geológicas, Facultad de Ciencias Exatas y Naturales, IGeBA Universidad de Buenos Aires, CONICET, Buenos Aires, Argentina

Abstract We conducted a magnetotelluric (MT) study from Paleoproterozoic Rio de la Plata Craton, in Uruguay, toward Paleozoic-Mesozoic Paraná Basin, in Brazil. The 850-km-long MT transect comprises 35 evenly spaced broadband electromagnetic soundings sites. In the Paraná Basin, 11 additional long-period measurements were acquired to extend the maximum depth of investigation. All data were inverted using two- and three-dimensional approaches obtaining the electrical resistivity structure from the surface down to 200 km. The Rio de la Plata Craton is >200-km thick and resistive (~2,000 Ωm). Its northern limit is electrically defined by a lithosphere scale lateral transition and lower crust conductive anomalies (1–10 Ωm) interpreted as a Paleoproterozoic suture at the southern edge of Rivera-Taquarembó Block. The latter is characterized by an approximately 100-km thick and moderate resistive (>500 Ωm) upper mantle. The Ibaré shear zone is another suture where an ocean-ocean subduction generated the 120-km thick and resistive (>1,000 Ωm) São Gabriel juvenile arc. Proceeding northward, a 70- to 80-km thick, 150-km wide, and inclined resistive zone is imaged. This zone could be remnant of an oceanic lithosphere or island arcs accreted at the southern border of Paraná Basin. The MT transect terminates within the southern Paraná Basin where a 150- to 200-km-thick less resistive lithosphere (<1,000 Ωm) may indicate refertilization processes during plate subduction and ocean closure in Neoproterozoic-Cambrian time. Our MT data support a tectonic model of NNE–SSW convergence for this segment of SW Gondwanaland.

1. Introduction

The tectonically stable part of the South American Plate comprises a set of Precambrian blocks welded together during orogenic events spanning from the Paleoproterozoic to the Neoproterozoic-Cambrian boundary (Almeida et al., 2000). However, large segments of Archean to Proterozoic South America basement are covered by a thick (up to 6 km) post-Cambrian volcano-sedimentary sequences which limit the reconstruction of the tectonic history of the South America platform. Therefore, geophysical data are essential to define the main tectonic units and their lithospheric properties.

Seismological studies using receiver function and surface wave tomography (e.g., Assumpcao et al., 2013; Feng et al., 2007; Rosa et al., 2016) indicate important variations in crustal thickness and upper mantle seismic velocities in the southern segment of the South American Plate. The thickest crust (38–46 km) is observed under the Paraná Basin, whereas the surrounding basins and cratons are characterized by a relatively thinner crust (30–35 km). A gravity study by Dragone et al. (2017) mapped a continental scale and elongated linear gravity feature which was interpreted as Neoproterozoic-Cambrian suture/shear zone on the western border of the Paraná Basin, the Western Paraná Suture/Shear Zone (WPS in Figure 1). WPS extends from the southern border of Amazon Craton and continues southward, separating the Paraná Basin from Rio Tebicuary and Rio de la Plata cratons (RPC; Figure 1). The gravity anomaly within WPS has an amplitude of 70 mGal, from positive Bouguer anomalies over the cratons to negative anomalies within the Paraná Basin. The main cause of this anomaly is the variation of crustal thickness (Dragone et al., 2017). However, on both sides of WPS, gravity data alone cannot discriminate tectonic blocks and terranes and their limits owing to the lack of significant lateral density contrast. Thus, we collected magnetotelluric (MT) data along an 850-km-long transect
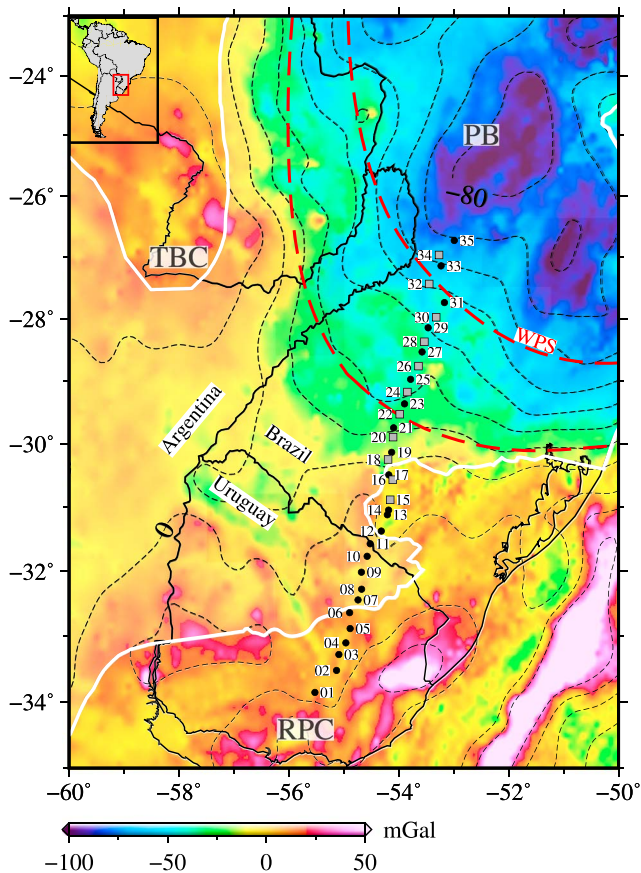
Figure 1. Magnetotelluric sites over Bouguer gravity anomalies upward continued to 30 km at 10-mGal contour interval (dashed black). Continuous white contours are the limits of the Paraná and Chaco-Paraná intracratonic basins. Continuous black contours are the political limits of countries. Numbers within white squares are magnetotelluric stations, black circles (broadband) and gray squares (long period). Dashed red lines are the limits of Western Paraná Suture/Shear Zone (WPS) after Dragone et al. (2017). RTC = Rio Tebicuary Craton, RPC = Rio de la Plata Craton, PB = Paraná Basin. Inset is the location of the study region (red rectangle) in South America.

perpendicular to WPS continental-scale gravity feature to estimate the electrical properties of cratons, terranes, and blocks involved in the suturing process. The MT transect starts in the center of Rio de la Plata Craton in Uruguay and extends toward the Paraná Basin. Additionally, the geoelectrical response was calibrated with the exposed Precambrian basement rocks, especially in Uruguay and south Brazil to help interpreting other buried electrical features under volcano and sedimentary rocks.

The MT method uses measurements of Earth's electromagnetic field time variations to determine the electrical resistivity distribution of Earth's interior. MT method has proven to be effective in defining terrane boundaries and relics of subduction and suture/shear zones in stable Precambrian areas, as attested by several MT studies in the Canadian and Fennoscandian shields (Jones et al., 2005; Korja et al., 2002). In the present study, the geoelectrical structure is investigated through two- and three-dimensional (2-D and 3-D) inversion of the MT data, providing electrical models of the deep crust and upper mantle. We used broadband (0.0001 to 3600 s) and long-period (10 to 13,600 s) MT soundings. The resistivity model allows us to map localized conductive features of Precambrian collision and subduction processes. The Rio de la Plata Craton thickness and lateral extension is electrically defined likewise the accreted terranes and blocks. To the north of Western Paraná Suture zone, the lithosphere is less resistive, most likely reflecting chemical alteration associated with fluid release and mantle edge processes in a subduction zone at the southern margin of the Paraná Basin. Finally, integrating the geological information with the electrical structure of the lithosphere along the MT transect a new tectonic model for the SW Gondwanaland formation is proposed and discussed.

2. A Geological Overview

The MT transect crosses the exposed basement of several tectonic units in Uruguay and Brazil (Figure 2). From south to north the main tectonic units are, in Uruguay, the Piedra Alta (Bossi et al., 1993) and the Nico Pérez (Bossi & Campal, 1992) terranes, which are separated by the Sarandí del Yí shear zone (Preciozzi et al., 1985). In Brazil, near the Uruguayan border, outcrops of Paleoproterozoic Taquarembó (Naumann et al., 1984) and Neoproterozoic São Gabriel blocks (Fragoso-Cesar, 1991) are found. The NW-SE trending Ibaré shear zone (IBSZ; Fragoso-Cesar, 1980) marks the transition from Paleoproterozoic units to the south and the juvenile (900–600 Ma) São Gabriel magmatic arc (Babinski et al., 1996) and ophiolites (Arena et al., 2016). Parallel and to the east of the MT transect is the Neoproterozoic to Cambrian Dom Feliciano fold and thrust belt (Fragoso-Cesar, 1980), which extends from southeastern Uruguay to latitude 27°S on the Brazilian Atlantic coast. On the western side of the MT transect is the southern extension of the Paraná basin with Paleozoic-Mesozoic sedimentary rocks and the Lower Cretaceous flood basalts. The northern edge of the MT transect is located near Chapecó city within the southern segment of the Paleozoic to Mesozoic Paraná basin, in the Brazilian territory (Figure 2). A review on the main geological aspects of the study area is presented below.

The Piedra Alta (PAT) and Nico Pérez terranes in Uruguay, the Buenos Aires Complex (Marchese & Di Paola, 1975) in Argentina and Taquarembó Block (south Brazil) altogether make the bulk of the RPC according to geological and tectonic studies reviewed by Almeida et al. (2000). More recently, Oyhantcabal et al. (2011), integrating geochronological, isotopic, and gravity data, redefined the RPC limits in Uruguay excluding from the craton the Nico Pérez Terrane and the Taquarembó Block.

The PAT is located to the west of Sarandí del Yi shear zone (Figure 2). It includes low- to medium-grade metamorphic orogenic belts and plutonic suites of tonalite–trondhjemite–granodiorite affinity (ca. 2.1 Ga), a
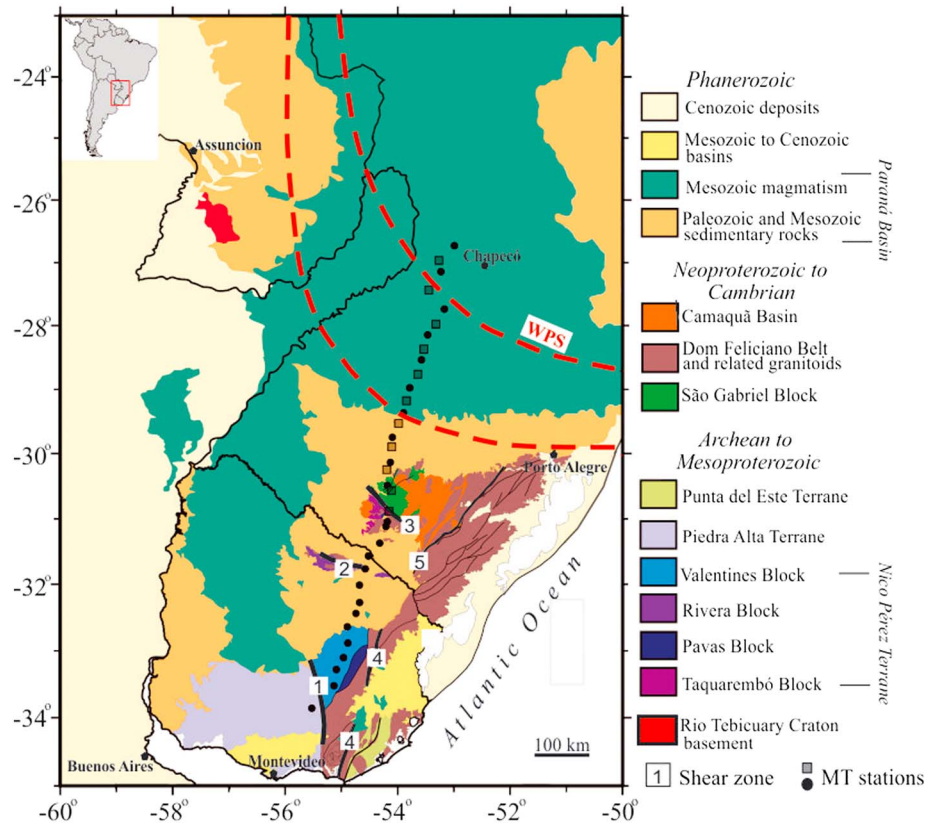
Figure 2. Main geological units in Uruguay and southern Brazil based on Preciozzi et al. (1985), Bartel et al. (1996), Bettucci et al. (2001), Wildner et al. (2008), and Oyhantcabal et al. (2011). Shear zones are as follows: (1) Sarandi-Yi, (2) Rivera, (3) Ibaré, (4) Serra Balena, and (5) Dorsal de Canguçu. Black circles (broadband) and gray squares (long period) are the magnetotelluric sites. Continuous black contours are the political limits of Brazil, Uruguay, Paraguay, and Argentina. Black diamonds are cities.

layered mafic complex, late to postorogenic magmatism (1.9–2.3 Ga), A-type-rapakivi granites (2.078 Ga), and an extensional magmatism (1.8 Ga) represented by the Florida mafic dyke swarm (Bossi & Cingolani, 2009; Hartmann et al., 2000; Oyhantcabal et al., 2011; Rapela et al., 2007; Sanchez Bettucci et al., 2010). According to Peel and Preciozzi (2006) PAT is a juvenile Palaeoproterozoic unit which has been tectonically stable since 1.8 Ga. The crust of the PAT is described (Oyhantcabal et al., 2011) as being generated in a single growth event based on Sm-Nd T_{DM} model ages between 2.8 and 2.3 Ga and crystallization ages at 2.2–2.1 Ga. Also, these authors propose that the terrane was already a thick and strong lithosphere by Neoproterozoic time.

The Nico Pérez Terrane (sensu Bossi & Campal, 1992; Sanchez Bettucci et al., 2010) is composed of different crustal blocks from Archean to Mesoproterozoic ages known as Valentines, Rivera, and Pavas. Unlike PAT, Nico Peréz Terrane was intensively affected by Neoproterozoic magmatism. Some authors (e.g., Malmann et al., 2007; Oyhantcabal et al., 2011) regard the Sierra Ballena shear zone as the eastern border of the Nico Pérez Terrane (Figure 2).

The Valentines Block (Preciozzi et al., 1985) is represented by granulitic gneisses, metapyroxenites, and magnetite-augite quartzites, intruded by Paleoproterozoic and Neoproterozoic magmatism. U-Pb sensitive high-resolution ion microprobe (SHRIMP) isotopic data obtained by Santos et al. (2003) on zircons suggested an age of 2163 ± 8 Ma for the protolith of the Valentines Block, and an age of 2058 ± 3 Ma for the high-grade metamorphism. Paleoproterozoic magmatism is represented by the anorogenic Illescas granitic batholith with Pb/Pb age of 1.75 Ga (Campal & Schipilov, 1995).

The Rivera Block (Preciozzi et al., 1985) is a high-grade, bimodal felsic-mafic association composed of mafic granulitic orthogneisses and supracrustal lithologies including banded iron formation, pyroxene

fels, and forsterite-bearing marbles. According to Oyhantcabal et al. (2011, 2012) the felsic granulitic orthogneisses are of high-K calc-alkaline nature, compatible with a continental magmatic arc setting. Also, Vidal (2009) indicates the metamorphic peak at 6–9 kbar and 800 °C for these granulites. U-Pb SHRIMP ages (Santos et al., 2003) indicated 2140 ± 6 Ma crystallization age and 2077 ± 6 Ma for high metamorphism of the felsic granulites.

The Pavas Block (Preciozzi et al., 1985) is represented by amphibolic gneisses, amphibolites, quartzites with fuchsite, and meta-ultramafic tremolite and actinolite schists. This block is intruded by Neoproterozoic magmatism such as Zapicán Diorite dated by U-Pb zircon ages of 610.4 ± 2.5 Ma by Oriolo et al. (2016). U-Pb (SHRIMP) analyses in zircons of a tonalitic orthogneiss (Hartmann et al., 2001) yielded ages of 3.41 Ga (core), interpreted as the crystallization age and from 3.1 to 2.7 Ga (rim) as metamorphic episodes.

According to Oyhantcabal et al. (2012) and Oriolo et al. (2016), the ages recorded in the different blocks of the Nico Pérez Terrane point to a multistage magmatism at ca. 2.18- to 2.10-Ga coeval with a high-grade metamorphism. Besides, Sm-Nd T_{DM} model ages indicate crustal growth at two distinct periods: 3.0–2.6 Ga and 2.3–1.6 Ga (Oyhantcabal et al., 2012). In addition, Oriolo et al. (2016) proposed that Nico Pérez Terrane was mostly generated during the Archean, and Hf T_{DM} distribution reveals Archean episodic crustal growth with main peaks of crustal generation during the Paleoarchean and Mesoarchean, indicating crustal reworking during the Proterozoic.

Further north, already within Brazil and separated by a large portion of basement capped by Phanerozoic sedimentary rocks, is the basement of Taquarembó Block, named Santa Maria Chico Granulitic Complex. These granulites represent a deep exposed crust composed of garnet-plagioclase clinopyroxene-orthopyroxene (quartz) rocks (Hartmann et al., 1999). This mineral association indicates ~10 kbar and 800 °C conditions and geochemical information suggests depletion in large ion lithophile elements. The protolith age is Paleoproterozoic of 2366 ± 8 Ma and 2489 ± 6 Ma ages by U-Pb SHRIMP according to Hartmann et al. (2008). Metamorphism was dated at 2.2–2.0 Ga by Hartmann et al. (1999) using U-Pb SHRIMP zircon ages. While the Rivera granulites have high-K calc-alkaline affinity, the Santa Maria Chico granulites are low-K calc-alkaline. Widespread Neoproterozoic granitic intrusions dated at 600–500 Ma (Hartmann & Nardi, 1982), likewise in the Rivera Block of Uruguay (Oyhantcabal et al., 2012), are observed in the Taquarembó Block. Based on the geographical proximity, geological similarities such as the age of protoliths and the degree of metamorphism, several authors suggested the correlation of these two granulitic areas (e.g., Basei et al., 2000; Fragoso-Cesar, 1991; Oyhantcabal et al., 2012).

Proceeding further north, the Ibaré shear zone (IBSZ in Figure 2) separates the Paleoproterozoic Taquarembó Block from the São Gabriel Block. Babinski et al. (1996), using U-Pb zircon dating of plutonic and volcanic rocks of Vila Nova belt, within the São Gabriel Block, proposed this belt to have formed between 750 and 700 Ma. Sm-Nd model ages range from 1000 to 800 Ma with positive ε_{Nd} (t) values. This result led the authors to propose a juvenile accretion due to an eastward subduction below the Paleoproterozoic RPC. Hartmann et al. (2011) set a time constraint of 753–680 Ma for the São Gabriel juvenile terrane accretion based on U-Pb SHRIMP zircon ages determined in granitic and metasedimentary rocks. Also, Saalmann et al. (2005) present T_{DM} Sm-Nd model ages on metamorphic volcano-sedimentary successions in the São Gabriel Block, indicating the existence of Meso-Neoproterozoic juvenile oceanic crust and island arc rocks at the border of the RPC. U-Pb zircon ages and Hf isotopic studies performed in the metaultramafic rocks (Arena et al., 2016) indicate a depleted mantle signature for the ophiolites and set the accretion between 1000 and 720 Ma.

Approximately at latitude 30.5°S, the MT transect reaches the southern erosional limit of the Paleozoic to Mesozoic Paraná basin. The basement of this intracratonic basin was dated by Cordani et al. (1984) as Paleoproterozoic (four samples), Mesoproterozoic (two samples), and Neoproterozoic (29 samples). Paraná magmatic province is one of the largest flood basalt provinces in the world (Bellieni et al., 1986; Peate, 1997) and the age of this magmatism is dated at ca. 135 Ma (Renne et al., 1992; Thiede & Vasconcelos, 2010) preceding the opening of the South Atlantic Ocean. The occurrence of this magmatism is almost entirely within the Paleozoic to Mesozoic Paraná basin (Milani & Ramos, 1998).

Finally, to the east of the MT transect and along the NE trending coastline is the Dom Feliciano belt. This belt represents the Brasiliano/Pan-African orogenic cycle (750–550 Ma; e.g., Fragoso-Cesar, 1980; Porada, 1989) in Uruguay and southern Brazil. It is genetically related to tectonic episodes that occurred during the

Neoproterozoic time with convergence of the Río de La Plata, Congo, and Kalahari cratons and the development of Kaoko, Gariep, and Damara Belts in southern Africa (see Dürr & Dingeldey, 1996 and references; Porada, 1989; Prave, 1996). Some authors (Gubert et al., 2016; Hartmann et al., 2011) regard the Dom Feliciano Belt as composed of lithological associations generated during São Gabriel (900–680 Ma) and Dom Feliciano (650–540 Ma) orogenic events. This belt extends for more than 1,000 km from southern Uruguay to Florianópolis city (−27°35′48″) in Brazil, being organized in three main units (Basei et al., 2000) from east to west: the granite belt (650–550 Ma), the schist belt (maximum Neoproterozoic age), and the foreland belt (Ediacarian age).

3. MT Data Processing and Modeling

3.1. Field Data

Five-component MT data (Ex, Ey, Hx, Hy, and Hz) were collected at 35 sites in the period range of 0.0001 to 3600 s with commercial broadband systems (Metronix ADU07) operating typically for 2 or 3 days. At 11 sites within the Paraná Basin, long-period data (10 to 13,600 s) were additionally acquired jointly with the Geomagnetism Group of Instituto Nacional de Pesquisas Espaciais using commercial equipment (Phoenix LRMT) operating for 3 or 4 weeks. These long-period soundings were undertaken to compensate the strong attenuation of the MT signal in the conductive sedimentary deposits of the Paraná Basin. The two components of the telluric field were measured with lead-lead chloride electrodes laid out in a cross with 150-m lengths. The three components of the magnetic field were measured with three individual high-sensitivity induction coils (broadband) or three-component fluxgate magnetometers (long-period).

The observed time series were processed using a robust remote reference code (Egbert, 1997), resulting in high-quality estimates of the impedance tensor and tipper vector, except for the dead band around 1–10 s in some sites. MT impedances and vertical field transfer functions for three representative sites are shown in Figure 3. Site 03 is located at the Valentines Block, in the southern part of the MT transect, where elevated values of apparent resistivity over the entire period range are observed. In the center of the MT transect, within the São Gabriel Block, site 13 also presents elevated resistivities. However, its responses are more variable, mainly at shorter periods. A decrease in the apparent resistivity amplitude, mainly in the yx mode, is attributed to the low signal-to-noise ratio MT signals from the dead band. Site 26 is within the Paraná Basin where responses are almost one-dimensional (1-D) at periods shorter than 100 s, and relatively conductive in all period range.

3.2. Induction Vectors

The vertical magnetic field transfer functions are given by the ratio of the vertical magnetic component to the horizontal magnetic components. They are usually displayed as induction vectors, which in the ideal 2-D case point perpendicularly to horizontal resistivity gradients. Figure 4 shows the induction vectors along the transect for periods of 6.4, 18, 585, and 1,170 s.

At short and intermediate periods, a well-defined reversal of the vectors is observed near site 08, suggesting the existence of an elongated conductor running approximately east-west. Such structure may be related to the Rivera Shear Zone, located just to the north of site 08, where the main foliation is approximately N70°W (Ellis, 1998). Regional anomalies from surface-wave group velocity data (Rosa et al., 2016) also trend approximately east-west in northern Uruguay.

In the central region, between sites 16 and 20, the vectors have a more complex behavior. They have relatively large amplitude and show off-transect components at 6.4- and 18-s periods, a possible indication of 3-D structure. As will be shown below from the decomposition analyses, for these stations there is an onset of 3-D effects between 1- and 10-s period. As stated by Jones et al. (1993), not only galvanic electric distortion effects would be expected near these periods but also 3-D induction and magnetic effects of galvanic charges. These effects will in general include a vertical magnetic field that adds to any vertical field caused by 2-D induction on a regional scale. Fortunately, these distorting effects are band limited and restricted to relatively shallow structures, as evidenced by the drastic reduction of both the amplitude and the off-profile component of the vectors at longer periods.

In the northern segment, almost all vectors are parallel to the MT transect, suggesting a 2-D regional structure with a strike nearly perpendicular to the transect. This strike is consistent with the local E-W trending linear
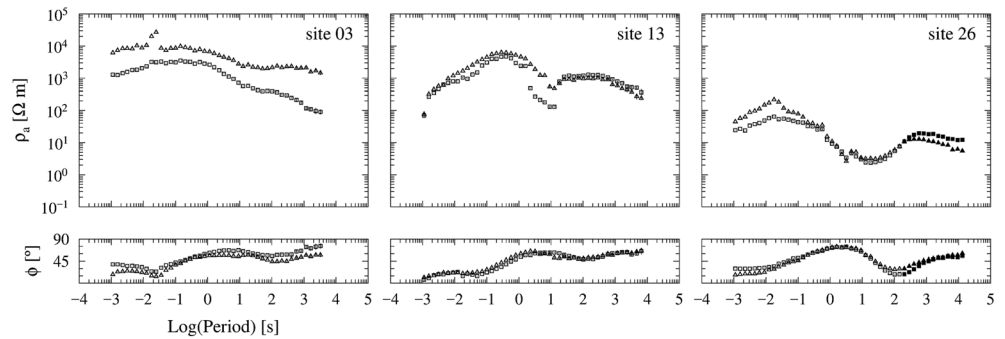
Figure 3. Apparent resistivity and phase of three representative sites with the *x* axis aligned with the geomagnetic north. Triangles and squares are the magnetotelluric responses from electric dipole oriented at N15°W and N75°E, respectively. Open symbols are data from broadband magnetotelluric system, while closed symbols are data from long-period system. Site 03 is located within the Valentines Block, in the southern part of the study area. Site 13 is representative of the São Gabriel Block, in the central part of the region. Site 26 shows a typical response for the volcano-sedimentary Paraná Basin.

gravity anomaly, which indicates a significant lateral variation of density (and composition) across the WPS suture zone.

At the southern end of the MT transect, the scenario is less clear because the vectors seem to be additionally influenced by a conductive structure located to the southeast of the transect, either within the Dom Feliciano Belt or in the offshore continental margin.

3.3. Dimensionality and Strike Analysis

Distorting effects of near-surface heterogeneities can lead to inaccurate determinations of strike directions and data dimensionality. To remove these effects, if existing, and to determine the impedances and strike of the regional 2-D geoelectrical structure, we applied a tensor decomposition (Groom & Bailey, 1989) to the data from all sites using McNeice and Jones (2001) algorithm. This code extended the Groom-Bailey approach to solve simultaneously for the best-fitting strike direction and values of the distortion parameters at multiple sites and for multiple periods.

Initially, the Groom-Bailey decomposition was applied to the data of each site allowing the strike and distortion parameters (twist and shear) to vary freely within one-decade-wide period bands. Figure 5 shows the derived strike directions, represented by bars, in the intervals of 1–10, 10–100, 100–1,000, and
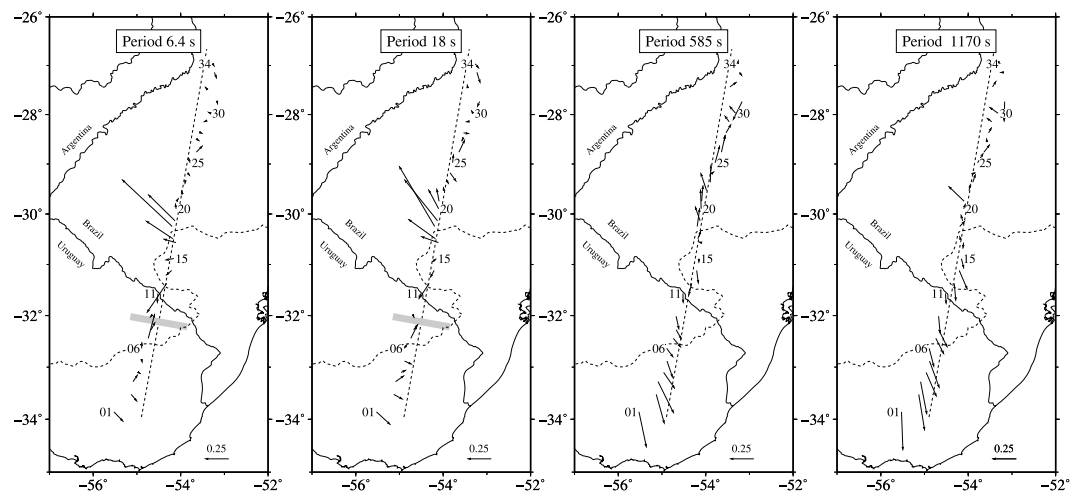
Figure 4. Real induction vectors of four representative periods using Parkinson convention. The gray-shaded zone is the location of a major reversion of induction vectors at intermediate periods. The dashed line is perpendicular to N80°W, the average strike direction (section 3.3). See text for details.
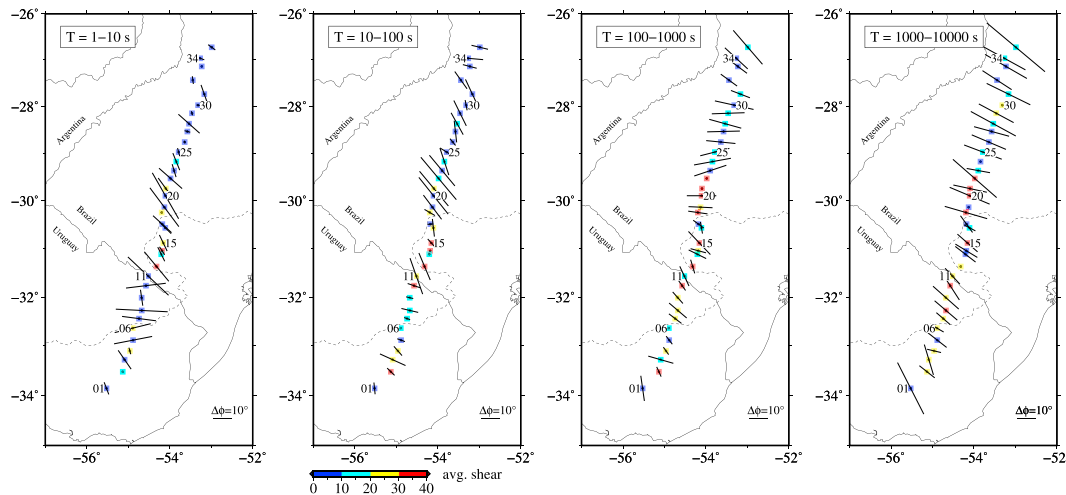
Figure 5. The unconstrained Groom-Bailey regional strike from four different period bands between 1 and 10,000 s. The orientation of the solid bars represents the estimated geoelectric strike direction for that period band, and the lengths of the bars are proportional to the average phase difference between the orthogonal directions. The colored squares show the average shear parameters.

1,000–10,000 s. Also shown, in colored squares, is the average shear distortion parameter for the respective band, which gives the relative degree of data distortion. Over each band, we have scaled the bars by the average phase difference between the off-diagonal elements of the recovered regional 2-D impedance tensor, thus providing a measure of the relative departure from the 1-D structure. In cases where the bars are small, the strike direction is of little importance because the MT responses do not change significantly with the coordinate system.

At the two shortest period bands (Figures 5a and 5b), most of the data present very small phase difference (<10°), implying in low order of multidimensionality. For those data with higher phase differences, the most consistent decomposition results are observed at the sites 11 to 23, in which the regional strikes have approximately the same value of N40°W to N50°W for both period bands. To the south, the strike azimuths at 1- to 10-s-period band for several sites (01–04 and 09) in the northern Uruguay differ significantly from east-west direction, which is evidence for the presence of strong 3-D distortions.

Further evidence for localized 3-D effects on the data set has been observed on a group of sites in the middle segment of the present MT transect. In these sites the strike and distortion parameters are strongly period-dependent, changing abruptly their values at periods around 0.1–10 s. From these periods on, there is a rapid increase in the twist and shear parameters beginning where the misfit is greatest. This effect is more pronounced at sites 17 to 22, where the induction vectors have off-transect components (as discussed on section 3.2), as well as at sites 10 to 12. According to Jones et al. (1993), this variation in the parameters means that we are moving from one 3-D/2-D regime at short periods (<10 s) to another 3-D/2-D regime at long periods (>10 s) through a regime in which a 3-D/2-D model is only an approximate description. Regional-scale 3-D distortions would become significant only at a few periods separating these two 3-D/2-D regimes.

At 100- to 1,000-s and 1,000- to 10,000-s-period bands, the regional strikes along the entire MT transect show a consistent preference for azimuths around N80°W.

Before proceeding to the data modeling, we calculated the most appropriate regional strike for the entire period range in each MT site, following the procedure described by Groom et al. (1993). Particularly, in stations where the strike azimuth abruptly changed with period, we gave preference for strike and distortion parameters from long periods, since this paper focuses on deep structures. By determining the arithmetic mean of the strike azimuths from all sites, an average value of N80°W was found. With the strike constrained to N80°W, we subsequently applied the Groom-Bailey decomposition to the data from all sites for the full period range. The model parameters and their fits for selected sites can be found in the Supporting Information S1.
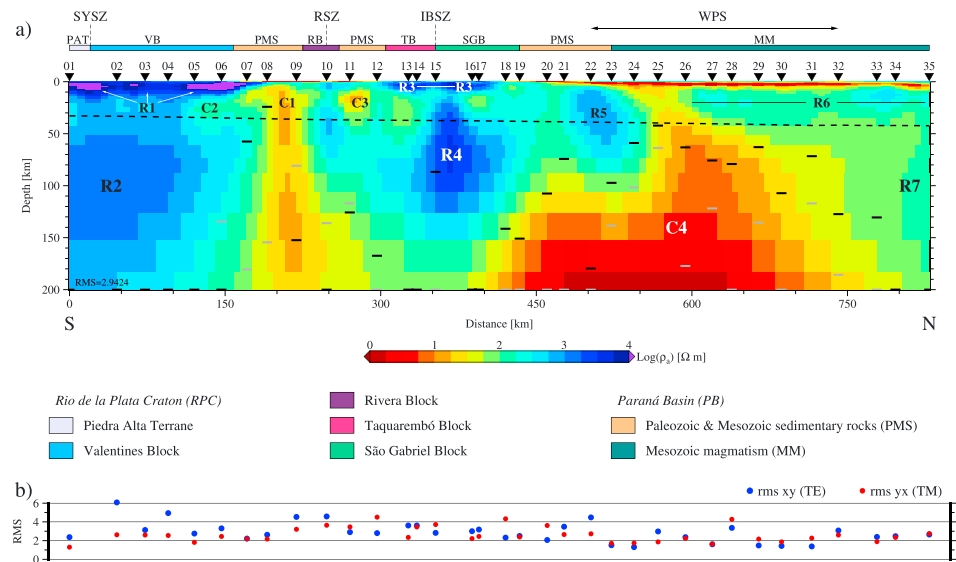
Figure 6. Two-dimensional resistivity model obtained by joint inversion of the TE and TM modes and correlation with the exposed or inferred geological information. Also shown is the computed normalized root-mean-square at each site along the transect. Black triangles are sites restricted to broadband data acquisition, while the red triangles are sites where both broadband and long-period MT systems were used. The dashed black line is the Moho depth based on Assumpcao et al. (2013). SYSZ = Sarandi Yi shear zone, RSZ = Rivera Shear Zone, IBSZ = Ibaré shear zone, and WPS = Western Paraná suture/shear zone. Gray and black bars are the maximum depth of investigation for the XY and YX modes, respectively, derived from the Niblett-Bostick transformation (a pseudo-section of the Niblett-Bostik transformation of the invariant impedances, Ingham, 1988, is shown in the supporting information). Bars plotted at the 250-km level have even deeper penetration. See text for discussion.

3.4. The 2-D Inversion

We first modeled the MT data using a 2-D inversion. The decomposed regional 2-D responses were inverted using REBOCC code (Siripunvaraporn & Egbert, 2000), which seeks minimum structure 2-D resistivity models. We run a series of inversions using different initial models, error floors, and subset of data. After decomposition of the impedance tensor, the xy and yx components were assigned to the TE and TM modes, which describe currents flowing parallel and perpendicular to strike (N80°W and N10°E, respectively). The TE and TM modes were inverted both individually and jointly. In all cases, we emphasized the phase over the apparent resistivity response, a standard procedure to account for static shift effects. Also, a small fraction of noisy data has been removed. Our final model (Figure 6) was derived from a joint TE and TM mode inversion with error floors set to 6% for phases (equivalent to 1.72°) and 15% for apparent resistivity values. The initial model consisted of a 450-Ωm half space. The resistivity model fits the observed data to a normalized root-mean-square (nrms) misfit of 2.94. The nrms values for individual stations (see Figure 6) indicate that the highest misfits occur at central and southern parts of the study area. These enhanced nrms values may be indicative of 3-D effects that cannot completely be modeled with 2-D inversion. The observed and predicted apparent resistivity and phase curves, are provided as supporting information.

An important feature of the inverse model is a subvertical zone (C1 in Figure 6) of low resistivity (~10 Ωm) beneath Paleozoic sedimentary rocks between the Valentines and Rivera blocks. The top of this feature is located near the depth of 5 km. Its base is not well defined, but probably C1 penetrates several tens of kilometers into the upper mantle, separating two electrically distinct lithospheres.

To the south of anomaly C1, both the upper crust and upper mantle are very resistive. The upper crust is imaged as ~10,000-Ωm zone (R1) with thickness of ~10 km beneath the PAT and most of the Valentines Block, decreasing to a few kilometers between sites 5 and 7. The northern edge of this resistive upper crust is underlain by a moderate conductor (C2), characterized by resistivity values of ~100 Ωm and a south dipping geometry. The remaining lower crust under the Valentines Block and PAT is relatively uniform and resistive (500–1000 Ωm). At upper mantle depths, a resistive (>1000 Ωm) root is observed down to

~200-km depth. The vertical extent of the deep root (R2) is poorly resolved, but it is reasonable to assume a lower boundary between 200 and 250 km, where a more pronounced decrease in resistivity is observed.

Immediately north of the anomaly C1, the overall geoelectrical structure is more complex than in the southern segment. A resistive upper crust (R3) also exists, but its thickness is far more variable, ranging from 5 to 10 km. The lower crust is imaged as a sequence of conductive (C3) and resistive (R3) bodies with resistivity values of about 10 and 1,000 Ωm, respectively. As in the southern model segment, the uppermost mantle (R4) is highly resistive (>1,000 Ωm). Yet below ~100 km the upper mantle resistivity decreases rapidly with depth.

Beneath the edge of the Paraná Basin, near the contact between the sedimentary and magmatic rocks of the Paraná Basin, an isolated ~500-Ωm body (R5) is observed. This ~75-km-wide feature makes up the entire crust in this area and extends to upper mantle depths (~70 km).

Most of the upper mantle under the southern border of the Paraná Basin in Brazil is underlain by a huge low-resistivity anomaly C4 (<10 Ωm). The depth to the top of this anomaly varies considerably; it is about 100 km in the southern part, it shallows abruptly to depths fewer than 40 km in the central part, and then it deepens gradually back to a 70-km depth in the north. Its base is not well resolved despite using long-period MT soundings.

Toward the northern Paraná Basin, the crust is imaged as a more homogeneous zone with resistivity ranging from 100 to 500 Ωm (R6). The underlying upper mantle to the north of site 32 also appears as a moderately resistive region (R7), which extends to depths about 150 km. These results are consistent with those of Padilha et al. (2015) for the central part of Paraná Basin.

To test if the anomalies C1 and C4 are required electrical sources, we run a set of sensitivity tests in which the lower part of these conductors was substituted by 100-Ωm blocks (see details in the supporting information). When limiting the depth extension of C1 to 220 km, the forward responses in its vicinity do not vary significantly. Instead, changes begin to occur only when the conductor depth is limited to 70 km, resulting in a downward bulge in the TE phase curve around 1,000 s. Regarding anomaly C4, limiting its depth extension to 220 km causes a significant deviation of the forward responses in respect to the inversion ones. This effect is more evident in the TE phase curve, which bends downward around the period of 10,000 s. Therefore, our sensitivity tests show that anomalies C1 and C4 are required electrical features in the 2-D model in order to adjust the observations.

3.5. The 3-D Inversion

The main motivation for carrying on 3-D electrical modeling of the subsurface is that the 2-D/3-D parameterization from the Groom-Bailey decomposition failed in some cases, mainly at the central and southern parts of the study area, which can lead to incorrect results if the data are modeled using 2-D inversion scheme. Despite that our data coverage is nonideal for 3-D modeling, several authors (Bologna et al., 2017; Kapinos et al., 2016; Meqbel et al., 2016; Patro & Egbert, 2011; Siripunvaraporn et al., 2005; Tietze & Ritter, 2013) have shown that application of 3-D inversion MT profile data can provide realistic images of the resistivity distribution beneath the data.

In this section, we applied the ModEM scheme of Kelbert et al. (2014) to model our data in 3-D. Adding the vertical field transfer functions data gives similar results (see Supporting Information S1). However, the impedance data misfits are larger in this case. Thus, we have given preference to the results derived from impedance-only inversions. Our preferred model was derived by inverting the full impedance tensor, assigning error floors of 5% of $\sqrt{(Z_{xy}Z_{yx})}$ to the four complex impedance tensor components. We used a 100-Ωm half space as prior model and 18 periods in the range between 0.1 to 13,000 s, after testing other values (50 and 500 Ωm). Data and model grid were rotated to N13°E. This value corresponds to the average azimuth of the MT transect, which is nearly perpendicular to the predominant geoelectrical strike direction of the survey area. All 35 stations were included, and inconsistent responses were removed. The study area was discretized into a 10-km grid in the core, padded with 12 cells on boundary with widths increasing by a factor of 1.3. Vertically, the 52 layers were used, starting with thickness of 25 m and increasing by a factor of 2. This discretization resulted in a 116 × 48 × 52 grid size in the x, y, and z directions. After 172 iterations, the inversion converged to an average nrms of 1.71.
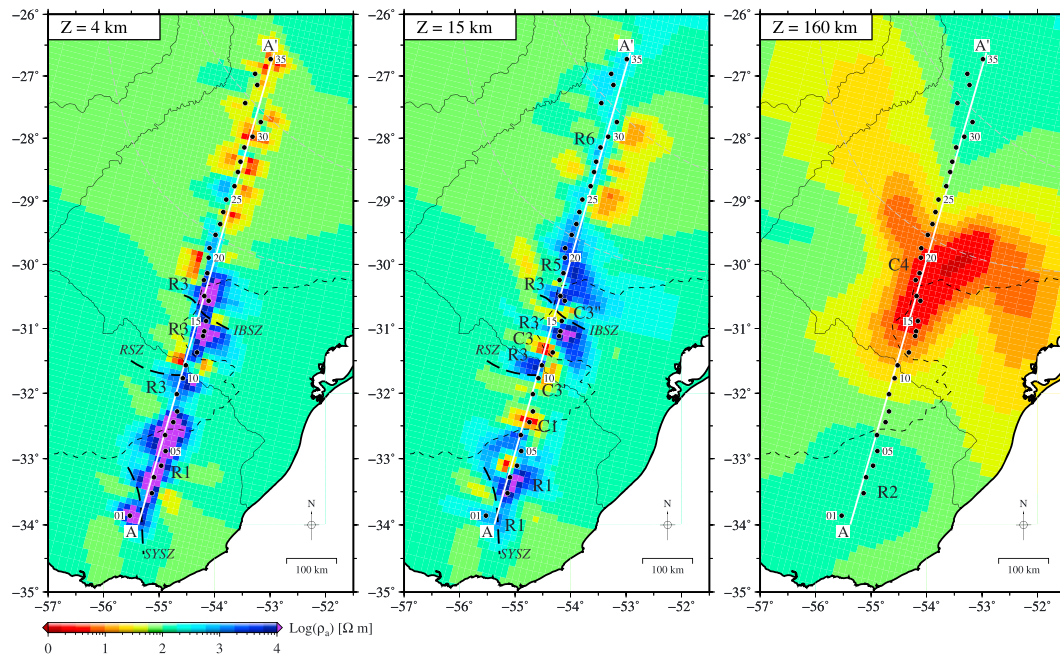
Figure 7. Three-dimensional inversion results shown in map view for three depths from crustal and upper mantle levels. Line A-A′ is a cross section extracted from the 3-D model (see Figure 8). The main anomalies are labeled as in Figure 6.

The results of the 3-D inversion are presented in Figures 7 and 8, which display depth sections of the preferred 3-D model at 4, 12, and 160 km and the vertical cross section extracted along the profile (line A-A′ in Figure 7c), respectively. Overall, the 3-D model fits the data very well, as shown in Figures 8b and 8c. The model responses for all 35 sites are provided as supporting information.

The deep and resistive lithosphere in the south end of the MT profile is also well defined in the 3-D model (Figure 8a), despite some differences. In comparison with the 2-D model, the highly resistive upper crust (R1) is slightly thicker, whereas the resistive mantle root (R2) is slightly shallower. Also, we observe a resistivity variation beneath the Sarandi Yi Shear Zone (SYSZ) at crustal depths, but we are uncertain if this variation is due to a fault or to a lack of horizontal resolution, given the large separation (~50 km) between sites 01 and 02. The position of the conductor C1 marking the northern limit of this lithospheric segment, has been slightly shifted to the south, moving from sites 08 and 09 to sites 07 and 08. In the 3-D model, this anomaly seems to penetrate only a few kilometers beyond the Moho depth.

In the central part of the survey area, the 3-D model displays closer correspondence between known shear zones and conductive features. While in the 2-D inversion the IBSZ had no associated electrical anomaly, in 3-D this zone coincides with a 10–30 Ωm crustal northward dipping anomaly (C3″ in Figure 8). The most significant difference between the 2-D and 3-D models occurs in the segment of the Paraná Basin. The isolated R5 resistive body shown in the 2-D model now consists of a strong northward dipping resistive zone (~10,000 Ωm) embedded in a ~1,000-Ωm layer with thickness of 50–70 km (R8). In addition, the prominent conductor C4 is imaged as a deeper feature (>100 km) and displaced southward in comparison with its position in the 2-D geoelectric model.

4. Discussion

In the following sections, we will discuss the results imaged in the 3-D inverse electrical model, as it better explains the observed data.

4.1. Electrical Structure of Rio de La Plata Craton

Among the tectonic units crossed by our MT transect, the PAT is the only tectonic unit that is generally agreed to be part of the RPC (Oyhantcabal et al., 2011; Peel & Preciozzi, 2006). As previously discussed, our results
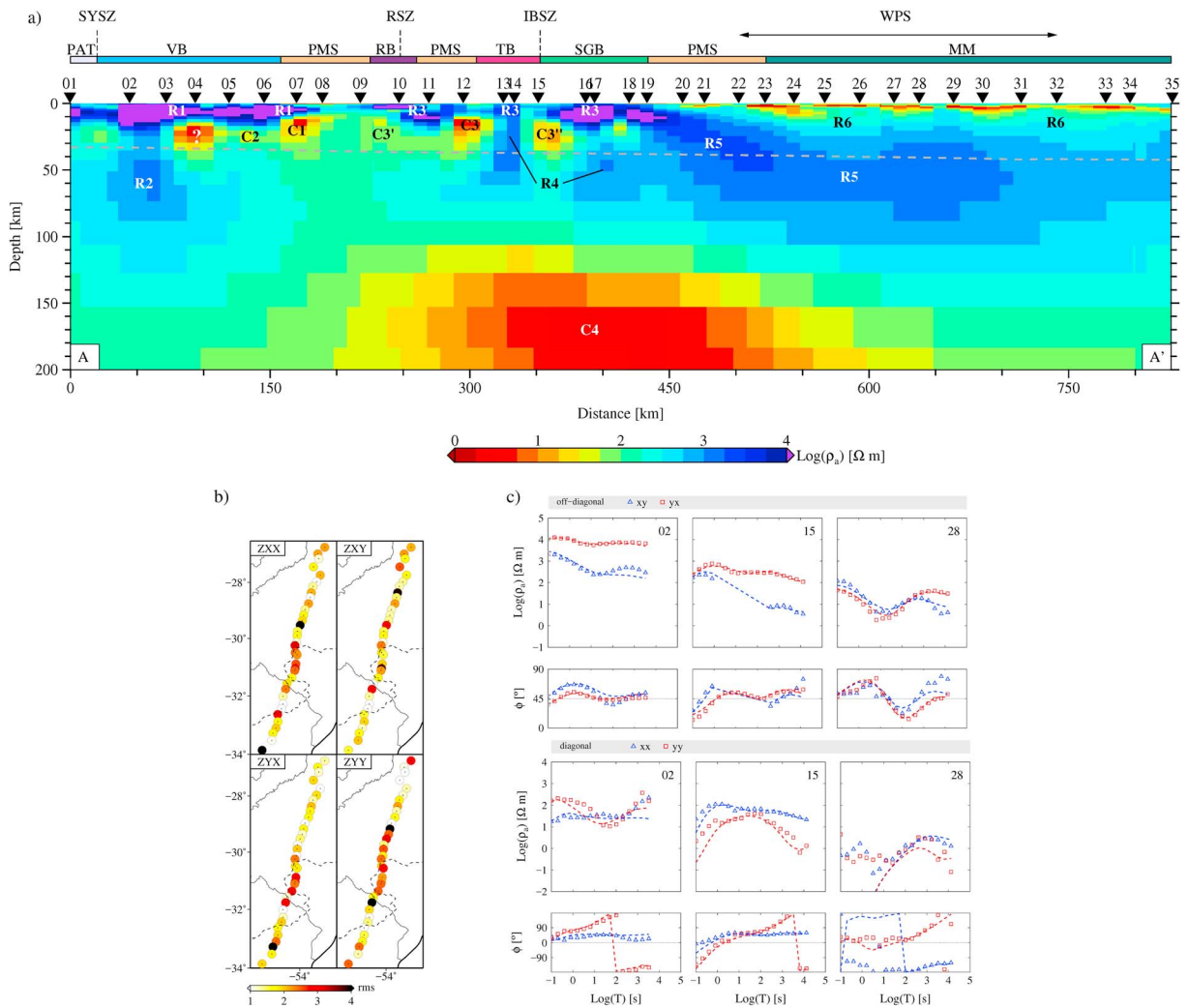
Figure 8. (a) Cross section extracted from the 3-D model along line A-A′ (see Figure 7). Geological information as in Figure 6. (b) Site-by-site distribution of the normalized root-mean-square averaged over 18 periods (0.01–13,000 s) for the four components of the impedance tensor. (c) Electrical responses for three representative sites. Acronyms at the top of the geoelectrical section as in Figure 6.

show that PAT, and most of the Valentines Block, is characterized by high-resistivity crust and upper mantle. The PAT resistivity structure is the eastern extension of the same electric lithosphere beneath the Chaco-Paraná Basin in central Argentina 500 km to the west of our study area. By inverting long-period MT data, Favetto et al. (2008) modeled the western border of the RPC as a highly resistive (up to 10,000 Ωm) keel extending from the crystalline basement of the Chaco-Paraná Basin down to 150- to 200-km depth.

The northeastern limit of the RPC has been a matter of debate (Rapela et al., 2007). A recent tectonic model (Oyhantcabal et al., 2011) considers this limit to be at the SYSZ. Recent geochronological and structural studies Oriolo et al., 2016 suggest that the Nico Pérez Terrane was accreted to the RPC at the end of the Neoproterozoic along the SYSZ. However, our results show no lithospheric-scale contrast in the electrical resistivity across the SYSZ. In fact, the overall resistivity structures of the Valentines Block and PAT are similar. The main exception is the northern border of the Valentines Block where a moderate resistivity (conductor C2) and another stronger feature are observed at lower crustal depths. But as commented by Meqbel et al. (2014), isolated conductive anomalies are commonly observed within cratonic areas.

Rather than the SYSZ, the northeastern limit of the RPC is marked by the conductor C1 (Figure 8). As a matter of comparison, one can refer to the MT data from EarthScope USArray program where Meqbel et al. (2014)

mapped several conductive zones separating major deep resistive blocks in the United States. One of the most prominent anomalies is the Cheyenne Belt conductor, a subvertical geological feature of low resistivity (<10 Ωm) between 25- and 60-km depth. This electrical feature lies in a shear zone that records the collision of a Proterozoic arc terrane with the Wyoming Craton. This electrical anomaly has been interpreted as caused either by major belts of graphitized biogenic material in metasedimentary rocks now deeply underthrust in Proterozoic sutures or by sulfides remobilized into fold hinges during deformation. We propose a similar interpretation for feature C1. Its age cannot be directly determined by the MT data, but given the age of ~2.1 Ga for the exhumed granulites in the Valentines, Rivera, and Taquarembó blocks, we propose that C1 was formed during the Paleoproterozoic collision of Rivera-Taquarembó Block with the eastern edge of the proto RPC comprising the PAT and Valentines Block.

The edge of this block might have undergone electrical change during tectonic processes from the Paleoproterozoic or later without remobilizing its deep root, hence preserving major cratonic properties. We infer that PAT and Valentines Block were already a single and stable tectonic unit probably since the Paleoproterozoic, implying that the SYSZ should be a relatively shallow shear zone. Its reactivation by the end of Neoproterozoic may be associated with the development of the Dom Feliciano Belt. The associated deformation and subsequent emplacement of granites along the SYSZ has not affected the mantle root under the PAT and Valentines Block. We conclude that the Valentines Block is an extension of the RPC.

4.2. Rivera-Taquarembó and São Gabriel Blocks

Further north the observed electrical anomalies might represent tectonic boundaries. The limit between the São Gabriel and Rivera-Taquarembó blocks, for example, corresponds to anomaly C3″ in our model (Figure 8). This crustal-scale conductor is located at the IBSZ. Because of the occurrence of 0.7- to 1.0-Ga ophiolites (Arena et al., 2016) along this shear zone, the C3″ feature may be associated with the NNE-SSW collision of the Rivera-Taquarembó and São Gabriel blocks during the Neoproterozoic. The tectonic scenario is less clear for the conductive anomaly (C3) underlying the Rivera and Taquarembó blocks because most of Precambrian basement in this region is covered by the sedimentary rocks of the Paraná basin. Given its similarity with features C3″ and C1, at São Gabriel Block and border of the RPC, the anomaly C3 may represent a cryptic (Paleoproterozoic?) contact between the Rivera and Taquarembó blocks. The anomaly associated with the Rivera Shear Zone (C3′ in Figure 8) is less intense and there is no significant lateral contrast in resistivity of the deep lithosphere north and south of this zone. Similarly to the SYSZ, we interpret the Rivera Shear Zone as a relatively shallow shear zone, whose deformation and subsequent emplacement of granites in Late Neoproterozoic has not affected the underlying mantle.

The bottom of resistor R4, taken at 100 Ωm, is located at approximately100-km depth, whereas in RPC this value is at 200-km depth. In order to decipher the nature of the low electrical resistivity mantle (feature C4 in Figure 8) under the Rivera-Taquarembó-São Gabriel blocks a local and higher-resolution seismic velocity model is required. Refertilized cratonic lithosphere predicts high to moderate P and S wave seismic velocities above the lithosphere-asthenosphere boundary, whereas for asthenospheric mantle a velocity reduction is expected below the lithosphere-asthenosphere boundary.

Within the Brazilian platform, an electrical anomaly (<10 Ωm at 130 km) equivalent to C4 is reported in the southern São Francisco Craton (SFC) by Pinto et al. (2010) and in the transition from SFC and the northern border of Paraná Basin by Bologna et al. (2011). This anomaly was interpreted as due to carbonatitic melts, at depths >80–100 km or carbon in the form of graphite deposited from carbonatitic melts within its stability depth (<100 km). The SFC strong electrical conductor correlates with Late Cretaceous Araxá kimberlite-carbonatitic complexes. At upper mantle condition, carbonate melt electrical conductivity is 5 orders of magnitude higher than that of the mantle olivine and 1 order of magnitude higher than basaltic melt, as experimentally determined by Gaillard et al. (2008) and Yoshino et al. (2010), respectively. Using a relationship between electrical conductivity and viscosity for the electrical anomaly in SFC, Sifré et al. (2015) estimated the presence of 0.03% to 0.2% of carbonate melt within a molten mantle. Using the Sigmelts software, Pommier and Le Trong (2011) estimated carbonatitic melt fraction of 0.2% at ~800 °C is predicted for resistivity of 10 Ωm, compatible with feature C4. Therefore, carbonatitic melts could be the source of anomaly C4 in Figure 8. Two undated carbonatites bodies within the Taquarembó Block and near IBSZ are reported by Toniolo et al. (2010) and Senhorinho (2012) and they may be the proxies of carbonatitic melts refertilization in the upper mantle during its evolution. Molten silicates as the cause of anomaly C4 is very

unlikely because high water content or an anomalously high temperature, not predicted by the Paraná Basin geotherm are required to onset peridotite melting.

4.3. The Paraná Cratonic Mantle

In Figure 7, as we move toward the north, the electrical structure of the lithosphere changes significantly. A large conductor (C4) is located at depths of 50–60 km, and because of its high conductivity the electromagnetic waves do not penetrate below 100 km. This anomaly coincides with Neoproterozoic-Cambrian WPS zone and former site of ocean closure and subduction (Dragone et al., 2017).

The cratonic nature of the Paraná Basin lithosphere is based on the Paleoproterozoic ages of its basement (Cordani et al., 1984; Milani & Ramos, 1998), the positive *P* and *S* velocity perturbations within a thick crust and lithospheric mantle (Feng et al., 2007 and Schaeffer & Lebedev, 2013) as well as normal heat flow values of 40–50 mW/m^2 (Hurter & Pollack, 1996). However, the apparent cratonic nature was recently challenged by Padilha et al. (2015) using electromagnetic induction study. The electrical resistivity of Paraná crust and upper mantle averages 500 Ωm, therefore lower than expected for Archean and Proterozoic cold, stable, and dehydrated cratons (Eaton et al., 2009) where highly electrically resistive (>10^3 Ωm) are usually expected and observed.

In the 2-D and 3-D models, the electrical structure imaged in the southern Paraná Basin indicates a lithosphere 150- to 200-km thick, but its deep crust (R6 in Figures 6 and 8) does not present a cratonic and electrical resistive character. To interpret R6 anomaly we follow the causative process proposed by Padilha et al. (2015), as Fe-enriched fluids impregnation during intense magmatic activity in Early Cretaceous leaving a conductive solid residue (sulfides or iron oxide, for instance) that altered the original cratonic nature of Paraná lithosphere.

The deep part of the Paraná lithosphere differs significantly in the 2-D and 3-D models. The 2-D model suggests an entire conductive lithosphere whereas the 3-D model indicates a resistive lithosphere for most of its upper mantle section. However, the northern segment of the MT profile is the part of the data set where the tensor decomposition and the induction vectors suggest that the 2-D approximation is acceptable. The 3-D inversion including other MT profiles in acquisition in the interior of the Paraná basin will allow us to determine the electrical structure of the lithosphere under the basin in a less ambiguous way.

A block of unknown affinity represented as R5? in the second tectonic section (top to bottom) in Figure 9 may be hidden under the border of Paraná Basin in southern Brazil. In the Canadian Shield, MT studies (e.g., Jones et al., 2005) have mapped a high-resistivity (>1,000 Ωm) region up to 60-km thick that has been interpreted as a microcontinent caught up in the Trans-Hudson orogen during the convergence of the Superior and Rae/Hearne Archean cratons. Similarly, we speculate that the resistor R5 (Figure 8) could be a continental fragment or an island arc that was accreted to the southern margin of the Paraná Basin lithosphere in the final amalgamation of the SW Gondwanaland.

Alternatively, the high resistive zone R5 could be a remnant of a former subduction zone beneath the Paraná Basin. MT studies in ancient and modern subduction settings have often imaged subducted oceanic plates as highly resistive slabs (Brasse et al., 2009; Jones, 1993; Kapinos et al., 2016). The enhanced resistivity is attributed to dehydrated lithosphere depleted of sediments (Wannamaker et al., 1989). Because of the dipping geometry and the proximity of R5 to a subduction setting, we consider the oceanic plate hypothesis as the most plausible explanation for R5 electrical resistor.

Proceeding further north in the electrical section of Figure 8, Paraná cratonic lithosphere becomes more conductive (<700 Ωm). Paraná lithosphere may have been refertilized at different extent as suggested by independent geochemical and geophysical observations. Re-Os isotopic determination for the Paraná basalts (Rocha-Júnior et al., 2012) from the northern and central Paraná magmatic province indicate asthenospheric metasomatic melt components generated at the mantle wedge during oceanic plate subduction. These melts were added to the Paraná lithospheric mantle. Depleted mantle metasomatized by pyroxenite and carbonatite melts was also proposed to explain the isotopic geochemistry of high-Ti basalts from southern Paraná magmatic province (Marques et al., 2018). The refertilization of an ancient depleted cratonic lithosphere due to metasomatic processes, by enrichment of Al, Ca, and Fe, increases the seismic velocities and density (Poudjom-Djomani et al., 2001). Indeed, *P* wave seismic tomography and positive density anomalies
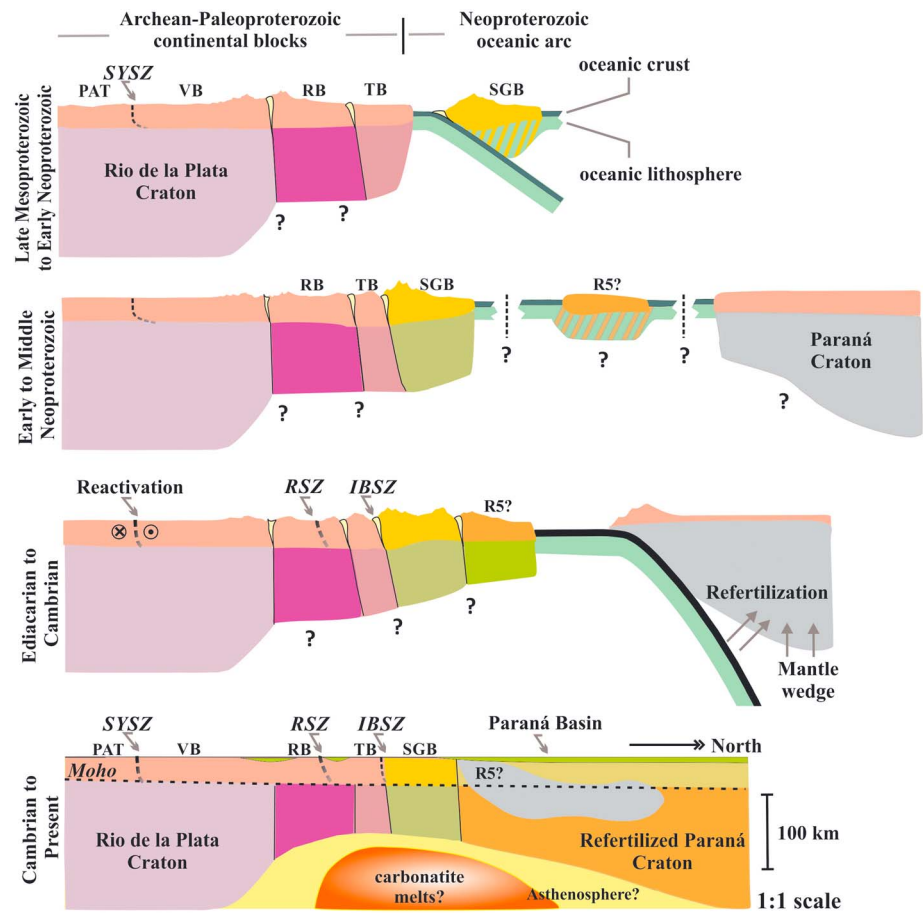
Figure 9. Proposed tectonic model integrating surface geology with electrical structure of the lithosphere (Figure 8). PAT = Piedra Alta terrane, VB=Valentines block, RB-TB = Rivera and Taquarembó blocks, SGB = São Gabriel juvenile oceanic arc, R5 = resistive block under Paraná Basin. Shear zones: SYSZ = Sarandi-Yi, RSZ = Rivera, IBSZ = Ibaré. "?" Marks are indicated where initial lithosphere thickness and width are unknown. For R5?, see text for detail.

from geoid inversion of Paraná lithosphere by Chaves et al. (2016) are consistent with a long-term refertilization process of subcontinental mantle lithosphere.

4.4. Proposed Tectonic Model

In Figure 9 the main geophysical results are summarized and integrated to propose a new tectonic model for SW Gondwanaland amalgamation. In the Late Mesoproterozoic-Early Neoproterozoic boundary (~1,0 Ga), the Rivera-Taquarembó Block was already accreted to the present northeastern border of the RPC (PAT and Valentines Block). During the Neoproterozoic (~700 Ma), the São Gabriel Block (SGB) collided with Rivera-Taquarembó Blocks (RB-TB) along the IBSZ. Question marks at the bottom of RB-TB and SGB blocks indicate that the thickness of the lithosphere in all sections are based on the present-day electrical lithosphere boundary assumed to be at resistivity <100 Ωm. A lithosphere fragment of unknown affinity, the electrical feature R5, converged to the margin of the SGB with subduction polarity toward the Paraná lithosphere. The final convergence and closure of the oceanic basin between the São Gabriel-R5 blocks and the Paraná lithosphere marked the final amalgamation of SW Gondwanaland in Neoproterozic-Cambrian time. From this time on, during the Paleozoic Paraná Basin subsided accumulating up to 5 km of sedimentary rocks (Milani & Ramos, 1998). In the Early Cretaceous this basin became one of the largest igneous provinces of the world due to melting of its refertilized lithospheric mantle (Marques et al., 2018; Rocha-Júnior et al., 2012). In the Late Cretaceous alkaline magmatism and carbonatites intruded the Paleozoic Paraná basin sedimentary sequences (Phillip et al., 2005).

5. Conclusions

We have mapped a resistive and thick lithosphere for the Rio de la Plata Craton. The resistivity structure indicates no geoelectrical contrast between Valentines Block and PAT across the SYSZ. The absence of conductors in the crust and in the mantle of this lithosphere implies that the lithosphere has not been significantly remobilized during the last thermotectonic events. Therefore, our results do not support significant reworking during Neoproterozoic or later events, including the one associated with the evolution of the Dom Feliciano belt. If the mapped resistive lithosphere corresponds to the RPC, then its northeastern border is well defined by crustal scale electrical and geological contact between the Valentines and Rivera-Taquarembó blocks, in central and central north Uruguay.

Detailed analyses of the regional geoelectrical strike suggest that lithospheric-scale deformations occurred along the WNW-SSE direction, implying a dominant NNE-SSW convergence for the tectonic units in the study area.

Our study suggests multiple accretion of terranes in the northeastern border of the RPC based on relative lateral variation of lithospheric thickness and electrical resistivity across the gravity-defined Western Paraná suture zone. The higher electrical conductivity of the northernmost Paraná lithosphere may be associated with metasomatic or refertilization processes within a mantle wedge between the lithospheric-asthenospheric boundary and fluid release from the top of a subducting oceanic plate during the convergence and collision of the Rio de la Plata Craton and its accreted terranes with the Paraná lithosphere since Neoproterozoic-Cambrian time.

References

Almeida, F. F. M., Neves, B. B. D., & Carneiro, C. D. (2000). The origin and evolution of the South American platform. *Earth Science Reviews*, *50*(1–2), 77–111. https://doi.org/10.1016/S0012-8252(99)00072-0

Arena, K. R., Hartmann, L. A., & Lana, C. (2016). Evolution of Neoproterozoic ophiolites from the southern Brasiliano Orogen revealed by zircon U-Pb-Hf isotopes and geochemistry. *Precambrian Research*, *285*, 299–314. https://doi.org/10.1016/j.precamres.2016.09.014

Assumpcao, M., Feng, M., Tassara, A., & Julia, J. (2013). Models of crustal thickness for South America from seismic refraction, receiver functions and surface wave tomography. *Tectonophysics*, *609*, 82–96. https://doi.org/10.1016/j.tecto.2012.11.014

Babinski, M., Chemale, F., Hartmann, L. A., vanSchmus, W. R., & daSilva, L. C. (1996). Juvenile accretion at 750-700 Ma in southern Brazil. *Geology*, *24*(5), 439–442. https://doi.org/10.1130/0091-7613(1996)024<0439:jaamis>2.3.co;2

Bartel, W., González, M., Muff, R., Lahner, L., & Wiens, F. (1996). Mapa Geológico de la República del Paraguay. Ministerio de Obras Públicas y Comunicaciones, MOPC e Instituto Federal de Geociencias y Recursos Naturales, BGR, Alemania, 1:100000 scale, Sheet: Paraguari 5459.

Basei, M., Siga, O., Masquelin, H., Harara, O., Reis Neto, J., & Preciozzi, F. (2000). The Dom Feliciano Belt of Brazil and Uruguay and its foreland domain, the Rio de la Plata Craton, framework, tectonic evolution and correlation with similar provinces of Southwestern Africa. In U. G. Cordani, E. J. Milani, A. Thomas-Filho, & D. A. Campos (Eds.), *Tectonic Evolution of South American Platform*, (pp. 311–334). Rio de Janeiro, RJ: International Union of Geological Sciences.

Bellieni, G., Comin-Chiaramonti, P., Marques, L. S., Melfi, A. J., Nardy, A. J. R., Papatrechas, C., et al. (1986). Petrogenetic aspects of acid and basaltic lavas from the Paraná plateau (Brazil): Geological, mineralogical and petrochemical relationships. *Journal of Petrology*, *27*(4), 915–944. https://doi.org/10.1093/petrology/27.4.915

Bettucci, L. S., Cosarinsky, M., & Ramos, V. S. (2001). Tectonic setting of the late Proterozoic Lavalleja group (Dom Feliciano Belt), Uruguay. *Gondwana Research*, *4*(3), 395–407. https://doi.org/10.1016/S1342-937X(05)70339-7

Bologna, M. S., Egbert, G. D., Padilha, A. L., Padua, M. B., & Vitorello, I. (2017). 3-D inversion of complex magnetotelluric data from an Archean-Proterozoic terrain in northeastern Sao Francisco Craton, Brazil. *Geophysical Journal International*, *210*(3), 1545–1559. https://doi.org/10.1093/gji/ggx261

Bologna, M. S., Padilha, A. L., Vitorello, I., & Pádua, M. B. (2011). Signatures of continental collisions and magmatic activity in Central Brazil as indicated by a magnetotelluric profile across distinct tectonic provinces. *Precambrian Research*, *185*(1-2), 55–64. https://doi.org/10.1016/j.precamres.2010.12.009

Bossi, J., & Campal, N. (1992). Magmatismo y tectónica transcurrente durante el Paleozoico inferior del Uruguay. In J. Gutiérrez, J. Saavedra, & I. Rábano (Eds.), *Paleozoico Inferior de Ibero – América*, (pp. 343–356). España: Universidad de Extremadura.

Bossi, J., & Cingolani, C. (2009). Extension and general evolution of the Río de la Plata craton. In C. Gaucher, A. N. Sial, G. P. Halverson, & H. E. Frimmel (Eds.), *Neoproterozoic-Cambrian Tectonics, Global Change and Evolution: A Focus on Southwestern Gondwana*, (pp. 73–85). Amsterdam, Netherlands: Elsevier.

Bossi, J., Preciozzi, F., & Campal, N. (1993). *Predevoniano en el Uruguay I: Terreno Piedra Alta, 1: 1–50, Dirección Nacional de Minería y Geología*. Uruguay: Montevideo.

Brasse, H., Kapinos, G., Mutschard, L., Alvarado, G. E., Worzewski, T., & Jegen, M. (2009). Deep electrical resistivity structure of northwestern Costa Rica. *Geophysical Research Letters*, *36*, L02310. https://doi.org/10.1029/2008gl036397

Campal, N., & Schipilov, A. (1995). The Illescas bluish quartz rapakivi granite (Uruguay-South America): some geological features. Paper presented at Symposium on Rapakivi granites and related rock, Belém, Brazil.

Chaves, C., Ussami, N., & Ritsema, J. (2016). Density and *P*-wave velocity structure beneath the Parana Magmatic Province: Refertilization of an ancient lithospheric mantle. *Geochemistry, Geophysics, Geosystems*, *17*, 3054–3074. https://doi.org/10.1002/2016gc006369

Cordani, U. G., Brito Neves, B. B., Fuck, R. A., Porto, R., Thomas-Filho, A., & Cunha, F. M. B. (1984). *Estudo preliminar de integração do pré-Cambriano com os eventos tectônicos das bacias sedimentares brasileiras, Série ciência-técnica-petroleo. Seçao, exploracão de petróleo.*

Publicação, (Vol. 15, pp. 20–27). Rio de Janeiro, Brasil: Petrobrás, Centro de Pesquisas e Desenvolvimento Leopoldo A. Miguez de Mello, Setor de Informação Técnica e Propriedade Industrial.

Dürr, S. B., & Dingeldey, D. P. (1996). The Kaoko belt (Namibia): part of a late Neoproterozoic continental-scale strike-slip system. *Geology*, *24*(6), 503–506. https://doi.org/10.1130/0091-7613(1996)024<0503:tkbnpo>2.3.co;2

Dragone, G. N., Ussami, N., Gimenez, M. E., Klinger, F. G. L., & Chaves, C. A. M. (2017). Western Parana suture/shear zone and the limits of Rio Apa, Rio Tebicuary and Rio de la Plata cratons from gravity data. *Precambrian Research*, *291*, 162–177. https://doi.org/10.1016/j.precamres.2017.01.029

Eaton, D. W., Darbyshire, F., Evans, R. L., Grütter, H., Jones, A. G., & Yuan, X. (2009). The elusive lithosphere–asthenosphere boundary (LAB) beneath cratons. *Lithos*, *109*(1-2), 1–2), 1–22. https://doi.org/10.1016/j.lithos.2008.05.009

Egbert, G. D. (1997). Robust multiple-station magnetotelluric data processing. *Geophysical Journal International*, *130*(2), 475–496. https://doi.org/10.1111/j.1365-246X.1997.tb05663.x

Ellis, J. H. D. (1998). The Precambrian of the "Isla Cristalina de Rivera" in northern Uruguay and their ore deposits, (PhD thesis), Heildelberg, Germany: University of Heildelberg

Favetto, A., Pomposiello, C., de Luchi, M. G. L., & Booker, J. (2008). 2D magnetotelluric interpretation of the crust electrical resistivity across the Pampean Terrane-Rio de la Plata suture, in Central Argentina. *Tectonophysics*, *459*(1–4), 54–65. https://doi.org/10.1016/j.tecto.2007.11.071

Feng, M., van der Lee, S., & Assumpção, M. (2007). Upper mantle structure of South America from joint inversion of waveforms and fundamental mode group velocities of Rayleigh waves. *Journal of Geophysical Research*, *112*, B04312. https://doi.org/10.1029/2006JB004449

Fragoso-Cesar, A. R. S. (1980). O Cráton do Rio de La Plata e o Cinturão Dom Feliciano no Escudo Uruguaio-Sul-Riograndense. Paper presented at 31°. Congresso Brasileiro de Geologia, Sociedade Brasileira de Geologia, Camboriú, Brazil.

Fragoso-Cesar, A. R. S (1991). Tectônica de placas no ciclo brasiliano: as orogenias dos cinturões Dom Feliciano e Ribeira no Rio Grande do Sul, (PhD thesis), São Paulo, SP: Universidade de São Paulo.

Gaillard, F., Malki, M., Iacono-Marziano, G., Pichavant, M., & Scaillet, B. (2008). Carbonatite melts and electrical conductivity in the asthenosphere. *Science*, *322*(5906), 1363–1365. https://doi.org/10.1126/science.1164446

Groom, R. W., & Bailey, R. C. (1989). Decomposition of magnetotelluric impedance tensors in the presence of local 3-dimensional galvanic distortion. *Journal of Geophysical Research*, *94*, 1913–1925. https://doi.org/10.1029/JB094iB02p01913

Groom, R. W., Kurtz, R. D., Jones, A. G., & Boerner, D. E. (1993). A quantitative methodology to extract regional magnetotelluric impedances and determine the dimension of the conductivity structure. *Geophysical Journal International*, *115*(3), 1095–1118. https://doi.org/10.1111/j.1365-246X.1993.tb01512.x

Gubert, M. L., Philipp, R. P., & Stipp Basei, M. A. (2016). The Bossoroca complex, Sao Gabriel terrane, Dom Feliciano Belt, southernmost Brazil: U-Pb geochronology and tectonic implications for the neoproterozoic Sao Gabriel arc. *Journal of South American Earth Sciences*, *70*, 1–17. https://doi.org/10.1016/j.jsames.2016.04.006

Hartmann, L. A., Campal, N., Santos, J. O. S., McNaughton, N. J., Bossi, J., Schipilov, A., & Lafon, J. M. (2001). Archean crust in the Rio de la Plata craton, Uruguay - SHRIMP U-Pb zircon reconnaissance geochronology. *Journal of South American Earth Sciences*, *14*(6), 557–570. https://doi.org/10.1016/s0895-9811(01)00055-4

Hartmann, L. A., Leite, J. A. D., McNaughton, N. J., & Santos, J. O. S. (1999). Deepest exposed crust of Brazil-SHRIMP establishes three events. *Geology*, *27*(10), 947–950. https://doi.org/10.1130/0091-7613(1999)027<0947:decobs>2.3.co;2

Hartmann, L. A., Liu, D., Wang, Y., Massone, H. J., & Santos, J. O. S. (2008). Protolith age of Santa Maria Chico granulites dated on zircons from an associated amphibolite-facies granodiorite in southernmost Brazil. *Anais da Academia Brasileira de Ciências*, *80*, 543–551. https://doi.org/10.1590/S0001-37652008000300014

Hartmann, L. A., & Nardi, L. V. S. (1982). Os Granitos Santo Afonso, Saibro e Vauthier da regiao de Dom Pedrito, RS: geologia, petrografia e geoquimica de elementos maiores, com interpretação geotectônica. *Acta Geologica Leopoldensia*, *12*, 153–178.

Hartmann, L. A., Philipp, R. P., Santos, J. O. S., & McNaughton, N. J. (2011). Time frame of 753–680 Ma juvenile accretion during the Sao Gabriel orogeny, southern Brazilian shield. *Gondwana Research*, *19*(1), 84–99. https://doi.org/10.1016/j.gr.2010.05.001

Hartmann, L. A., Pineyro, D., Bossi, J., Leite, J. A. D., & McNaughton, N. J. (2000). Zircon U-Pb SHRIMP dating of Palaeoproterozoic Isla Mala granitic magmatism in the Rio de la Plata craton, Uruguay. *Journal of South American Earth Sciences*, *13*(1–2), 105–113. https://doi.org/10.1016/s0895-9811(00)00018-3

Hurter, S. J., & Pollack, H. N. (1996). Terrestrial heat flow in the Paraná Basin, southern Brazil. *Journal of Geophysical Research*, *101*, 8659–8671. https://doi.org/10.1029/95JB03743

Ingham, M. (1988). The use of invariant impedances in magnetotelluric interpretation. *Geophysical Journal*, *92*(1), 165–169. https://doi.org/10.1111/j.1365-246X.1988.tb01130.x

Jones, A. G. (1993). Electromagnetic images of modern and ancient subduction zones. *Tectonophysics*, *219*(1–3), 29–45. https://doi.org/10.1016/0040-1951(93)90285-r

Jones, A. G., Groom, R. W., & Kurtz, R. D. (1993). Decomposition and modelling of the BC87 dataset. *Journal of Geomagnetism and Geoelectricity*, *45*(9), 1127–1150. https://doi.org/10.5636/jgg.45.1127

Jones, A. G., Ledo, J., & Ferguson, I. J. (2005). Electromagnetic images of the Trans-Hudson Orogen: The North American Central Plains anomaly revealed. *Canadian Journal of Earth Sciences*, *42*(4), 457–478. https://doi.org/10.1139/e05-018

Kapinos, G., Montahaei, M., Meqbel, N., & Brasse, H. (2016). Three-dimensional electrical resistivity image of the south-central Chilean subduction zone. *Tectonophysics*, *666*, 76–89. https://doi.org/10.1016/j.tecto.2015.10.016

Kelbert, A., Meqbel, N., Egbert, G. D., & Tandon, K. (2014). ModEM: A modular system for inversion of electromagnetic geophysical data. *Computational Geosciences*, *66*, 40–53. https://doi.org/10.1016/j.cageo.2014.01.010

Korja, T., Engels, M., Zhamaletdinov, A. A., Kovtun, A. A., Palshin, N. A., Smirnov, M. Y., et al., & BEAR Working Group (2002). Crustal conductivity in Fennoscandia—A compilation of a database on crustal conductance in the Fennoscandian shield. *Earth, Planets and Space*, *54*(5), 535–558.

Malmann, G., Chemale, F. Jr., Avila, J. N., Kawashita, K., & Armstrong, R. A. (2007). Isotope geochemistry and geochronology of the Nico Perez terrane, Rio de la Plata craton, Uruguay. *Gondwana Research*, *12*(4), 489–508. https://doi.org/10.1016/j.gr.2007.01.002

Marchese, H. G., & Di Paola, E. (1975). Miogeosinclinal Tandil. *Revista de la Asociación Geológica Argentina*, *30*(2), 161–179.

Marques, L. S., De Min, A., Rocha, E. R. V., Babinski, M., Bellieni, G., & Figueiredo, A. M. G. (2018). Elemental and Sr-Nd-Pb isotope geochemistry of the Florianopolis Dyke Swarm (Parana Magmatic Province): crustal contamination and mantle source constraints. *Journal of Volcanology and Geothermal Research*, *355*, 149–164. https://doi.org/10.1016/j.jvolgeores.2017.07.005

McNeice, G. W., & Jones, A. G. (2001). Multisite, multifrequency tensor decomposition of magnetotelluric data. *Geophysics*, *66*(1), 158–173. https://doi.org/10.1190/1.1444891

Meqbel, N., Weckmann, U., Munoz, G., & Ritter, O. (2016). Crustal metamorphic fluid flux beneath the Dead Sea basin: Constraints from 2-D and 3-D magnetotelluric modelling. *Geophysical Journal International*, *207*(3), 1609–1629. https://doi.org/10.1093/gji/ggw359

Meqbel, N. M., Egbert, G. D., Wannamaker, P. E., Kelbert, A., & Schultz, A. (2014). Deep electrical resistivity structure of the northwestern US derived from 3-D inversion of USArray magnetotelluric data. *Earth and Planetary Science Letters*, *402*, 290–304. https://doi.org/10.1016/j.epsl.2013.12.026

Milani, E. J., & Ramos, V. S. (1998). Orogenias paleózoicas no domínio sul-ocidental do Gondwana e os ciclos de subsidência da Bacia do Paraná. *Revista Brasileira de Geociencias*, *28*(4), 527–544.

Naumann N. P., Hartmann, L.A., Koppe, J.C., & Chemale-Jr, F. (1984). Seqüências supracrustais, ganisses graníticos, granulitos e granitos intrusivos da região de Ibaré-Palma, RS - Geologia, Aspectos estratigáficos e considerações geotectônicas. Paper presented at 33°. Congresso Brasileiro de Geologia, Sociedade Brasileira de Geologia, Rio de Janeiro, Brazil.

Oriolo, S., Oyhantcabal, P., Wemmer, K., Basei, M. A. S., Benowitz, J., Pfaender, J., et al. (2016). Timing of deformation in the Sarandi del Yi Shear Zone, Uruguay: Implications for the amalgamation of western Gondwana during the Neoproterozoic Brasiliano-Pan-African Orogeny. *Tectonics*, *35*, 754–771. https://doi.org/10.1002/2015tc004052

Oyhantcabal, P., Siegesmund, S., & Wemmer, K. (2011). The Rio de la Plata craton: A review of units, boundaries, ages and isotopic signature. *International Journal of Earth Sciences*, *100*(2–3), 201–220. https://doi.org/10.1007/s00531-010-0580-8

Oyhantcabal, P., Wagner-Eimer, M., Wemmer, K., Schulz, B., Frei, R., & Siegesmund, S. (2012). Paleo- and Neoproterozoic magmatic and tectonometamorphic evolution of the Isla Cristalina de Rivera (Nico Perez terrane, Uruguay). *International Journal of Earth Sciences*, *101*(7), 1745–1762. https://doi.org/10.1007/s00531-012-0757-4

Padilha, A. L., Vitorello, I., Antunes, C. E., & Padua, M. B. (2015). Imaging three-dimensional crustal conductivity structures reflecting conti-nental flood basalt effects hidden beneath thick intracratonic sedimentary basin. *Journal of Geophysical Research: Solid Earth*, *120*, 4702–4719. https://doi.org/10.1002/2014JB011657

Patro, P. K., & Egbert, G. D. (2011). Application of 3D inversion to magnetotelluric profile data from the Deccan Volcanic Province of Western India. *Physics of the Earth and Planetary Interiors*, *187*(1-2), 33–46. https://doi.org/10.1016/j.pepi.2011.04.005

Peate, D. W. (1997). The Paraná-Etendeka Province. In J. J. Mahoney & M. E. Coffin (Eds.), *Large igneous provinces in continental, oceanic and planetary flood volcanism, Geophys. Monogr. Series* (Vol. 100, pp. 217–245). Washington DC: American Geophysical Union.

Peel, E., & Preciozzi, F. (2006). Geochronologic synthesis of the Piedra Alta Terrane, Uruguay. Paper presented at V South American Symposium on Isotope Geology, Punta del Este, Uruguay.

Phillip, R., Vieiro, A. P., Comin-Chiaramonti, P., & Gomes, C. B. (2005). Mesozoic alkaline rocks of Rio Grande do Sul. In P. Comin-Chiaramonti & C. B. Gomes (Eds.), *Mesozoic to Cenozoic Alkaline Magmatism in the Brazilian Platform* (pp. 573–590). São Paulo, SP: Editora da Universidade de São Paulo-FAPESP.

Pinto, L. G. R., Pádua, M. B., Ussami, N., Vitorello, I., Padilha, A. L., & Braitenberg, C. (2010). Magnetotelluric deep soundings, gravity and geoid in the south Sao Francisco craton: Geophysical indicators of cratonic lithosphere rejuvenation and crustal underplating. *Earth and Planetary Science Letters*, *297*(3–4), 423–434. https://doi.org/10.1016/j.epsl.2010.06.044

Pommier, A., & Le Trong, E. (2011). SIGMELTS: A web portal for electrical conductivity calculations in geosciences. *Computational Geosciences*, *37*(9), 1450–1459. https://doi.org/10.1016/j.cageo.2011.01.002

Porada, H. (1989). Pan-African rifting and Orogenesis in southern to equatorial Africa and eastern Brazil. *Precambrian Research*, *44*(2), 103–136. https://doi.org/10.1016/0301-9268(89)90078-8

Poudjom-Djomani, Y. H., O'Reilly, S. Y., Griffin, W. L., & Morgan, P. (2001). The density structure of subcontinental lithosphere through time. *Earth and Planetary Science Letters*, *184*(3–4), 605–621. https://doi.org/10.1016/S0012-821X(00)00362-9

Prave, A. R. (1996). Tale of three cratons: Tectonostratigraphic anatomy of the Damara orogen in northwestern Namibia and the assembly of Gondwana. *Geology*, *24*(12), 1115–115. https://doi.org/10.1130/0091-7613(1996)024<1115:totcta>2.3.co;2

Preciozzi, F., Spoturno, J., Heinzen, W., & Rossi, P. (1985). *Carta Geológica del Uruguay (scale 1:500,000)*. Montevideo, Uruguay: DINAMIGE.

Rapela, C. W., Pankhurst, R. J., Casquet, C., Fanning, C. M., Baldo, E. G., González-Casado, J. M., et al. (2007). The Rio de la Plata craton and the assembly of SW Gondwana. *Earth Science Reviews*, *83*(1–2), 49–82. https://doi.org/10.1016/j.earscirev.2007.03.004

Renne, P., Ernesto, M., Pacca, I. G., Coe, R. S., Prévot, M., & Perrin, M. (1992). The age of Paraná flood volcanism, rifting of Gondwanaland, and the Jurassic-Cretaceous boundary. *Science*, *258*(5084), 975–979. https://doi.org/10.1126/science.258.5084.975

Rocha-Júnior, E. R. V., Puchtel, I. S., Marques, L. S., Walker, R. J., Machado, F. B., Nardy, A. J. R., et al. (2012). Re-Os isotope and highly siderophile element systematics of the Parana continental flood basalts (Brazil). *Earth and Planetary Science Letters*, *337-338*, 164–173. https://doi.org/10.1016/j.epsl.2012.04.050

Rosa, M. L., Collaco, B., Assumpcao, M., Sabbione, N., & Sanchez, G. (2016). Thin crust beneath the Chaco-Parana Basin by surface-wave tomography. *Journal of South American Earth Sciences*, *66*, 1–14. https://doi.org/10.1016/j.jsames.2015.11.010

Saalmann, K., Hartmann, L. A., Remus, M. V. D., Koester, E., & Conceicao, R. (2005). Sm-Nd isotope geochemistry of metamorphic volcano-sedimentary successions in the Sao Gabriel block, southernmost Brazil: Evidence for the existence of juvenile Neoproterozoic oceanic crust to the east of the Rio de la Plata craton. *Precambrian Research*, *136*(2), 159–175. https://doi.org/10.1016/j.precamres.2004.10.006

Sanchez Bettucci, L., Peel, E., & Masquelin, H. (2010). Neoproterozoic tectonic synthesis of Uruguay. *International Geology Review*, *52*(1), 51–78. https://doi.org/10.1080/00206810903358095

Santos, J. O. S., Hartmann, L. A., Bossi, J., Campal, M., Schipilov, A., Pineyro, D., & McNaughton, N. J. (2003). Duration of the trans-Amazonian cycle and its correlation within South America based on U-Pb SHRIMP geochronology of the La Plata craton, Uruguay. *International Geology Review*, *45*(1), 27–48. https://doi.org/10.2747/0020-6814.45.1.27

Schaeffer, A. J., & Lebedev, S. (2013). Global shear-speed structure of the upper mantle and transition zone. *Geophysical Journal International*, *194*(1), 417–449. https://doi.org/10.1093/gji/ggt095

Senhorinho, E.M. (2012). Controle estrutural dos carbonatitos no Rio Grande do Sul: análise de produtos de sensoriamento remoto e aerogeofísico. (BSc Dissertation). Retrieved from http://hdl.handle.net/10183/66113. Porto Alegre, RS: Universidade Federal do Rio Grande do Sul.

Sifré, D., Hashim, L., & Gaillard, F. (2015). Effects of temperature, pressure and chemical compositions on the electrical conductivity of car-bonated melts and its relationship with viscosity. *Chemical Geology*, *418*, 189–197. https://doi.org/10.1016/j.chemgeo.2014.09.022

Siripunvaraporn, W., & Egbert, G. (2000). An efficient data-subspace inversion method for 2-D magnetotelluric data. *Geophysics*, *65*(3), 791–803. https://doi.org/10.1190/1.1444778

Siripunvaraporn, W., Egbert, G., & Uyeshina, M. (2005). Interpretation of two-dimensional magnetotelluric profile data with three-dimensional inversion: Synthetic examples. *Geophysical Journal International*, *160*(3), 804–814. https://doi.org/10.1111/j.1365-246X.2005.02527.x

Thiede, D. S., & Vasconcelos, P. M. (2010). Paraná flood basalts: Rapid extrusion hypothesis confirmed by new 40Ar/39Ar results. *Geology*, *38*(8), 747–750. https://doi.org/10.1130/G30919.1

Tietze, K., & Ritter, O. (2013). Three-dimensional magnetotelluric inversion in practice-the electrical conductivity structure of the San Andreas fault in Central California. *Geophysical Journal International*, *195*(1), 130–147. https://doi.org/10.1093/gji/ggt234

Toniolo, J. A., Parisi, G. N., Grazia, C. A., & Reischl, J. L. 2010. Prospecção de fosfato na área de Três Estradas, Lavras do Sul, *RS* Paper presented 4th Simpósio Brasileiro de Exploração Mineral, ADIMB, Ouro Preto, Brazil.

Vidal, H. (2009). Estudio geológico-estructural del área de Cerro Papagayo, Isla Cristalina de Rivera-Uruguay. (Ph Thesis), Montevideo: Universad de la República.

Wannamaker, P. E., Booker, J. R., Jones, A. G., Chave, A. D., Filloux, J. H., Waff, H. S., & Law, L. K. (1989). Resistivity cross section through the Juan de Fuca subduction system and its tectonic implications. *Journal of Geophysical Research*, *94*, 14,127–14,144. https://doi.org/10.1029/JB094iB10p14127

Wildner, W., Ramgrab, G. E., Lopes, R. D., & Iglesias, C. D. F. (2008). Mapa Geológico do Estado do Rio Grande do Sul, 1:750.000 scale, Companhia de Pesquisa de Recursos Minerais, Ministério de Minas e Energia, Porto Alegre.

Yoshino, T., Laumonier, M., McIsaac, E., & Katsura, T. (2010). Electrical conductivity of basaltic and carbonatite melt-bearing peridotite at high-pressures: Implications for melt distribution and melt fraction in the upper mantle. *Earth and Planetary Science Letters*, *295*(3-4), 593–602. https://doi.org/10.1016/j.epsl.2010.04.050